Journal of Luminescence 132 (2012) 1257–1260

Contents lists available at SciVerse ScienceDirect

Journal of Luminescence

journal homepage: www.elsevier.com/locate/jlumin

Crystal structure and luminescence properties of Lu^{3+} and Mg^{2+} incorporated silicate garnet $[Ca_{3-(x+0.06)}Lu_xCe_{0.06}](Sc_{2-y}Mg_y)Si_3O_{12}$

Yongfu Liu [a,b], Xia Zhang [a,*], Zhendong Hao [a], Yongshi Luo [a], XiaoJun Wang [c], Jiahua Zhang [a,*]

[a] State Key Laboratory of Luminescence and Applications, Changchun Institute of Optics, Fine Mechanics and Physics, Chinese Academy of Sciences, 3888 Eastern South Lake Road, Changchun 130033, China
[b] Graduate School of Chinese Academy of Sciences, Beijing 100039, China
[c] Department of Physics, Georgia Southern University, Statesboro, GA 30460, United States

ARTICLE INFO

Article history:
Received 8 July 2011
Received in revised form
7 December 2011
Accepted 21 December 2011
Available online 30 December 2011

Keywords:
Lu^{3+}–Mg^{2+}
Ce^{3+} luminescence
Phosphor
White LED

ABSTRACT

The yellow-emitting phosphor $[Ca_{3-(x+0.06)}Lu_xCe_{0.06}](Sc_{2-y}Mg_y)Si_3O_{12}$ obtained from Lu^{3+} and Mg^{2+} co-modified green-emitting silicate garnet $Ca_3Sc_2Si_3O_{12}:Ce^{3+}$ (CSS:Ce^{3+}) exhibits promising applications for white LEDs. In this paper, we discuss the effect of charge balance on the garnet structure formation. The changes of bond length and covalence caused by the replacement of Lu^{3+} and Mg^{2+} for Ca^{2+} and Sc^{3+} are analyzed. The shift of the Ce^{3+} emission and excitation can be attributed to the combined results from crystal field splitting effect and centroid shift of Ce^{3+} 5d levels. Thermal stability is analyzed according to configurational coordinate diagram.

1. Introduction

Phosphor converted white light emitting diode (pcWLED) is regarded as a new lighting source for the next generation [1,2]. The most current pcWLEDs employ yellow-emitting $Y_3Al_5O_{12}:Ce^{3+}$ (YAG:Ce^{3+}) garnet phosphors combined with blue InGaN LEDs [3,4]. The YAG:Ce^{3+} emits a yellow band peaking at 530 nm with a width of about 100 nm due to $5d\rightarrow{}^2F_{7/2}$, $^2F_{5/2}$ transition [5]. The deficient red emission leads to the color rendering index (CRI) of white LEDs being below 80. To enrich the red emission, significant investigations have been done to modify YAG:Ce^{3+} by substitutions for Y^{3+} and Al^{3+} sites [6–8].

In addition to Al-based garnets, a new green-emitting silicate garnet phosphor $Ca_3Sc_2Si_3O_{12}:Ce^{3+}$ (CSS:Ce^{3+}) suitable for blue excitation has attracted much attention for its higher luminescence and higher thermal stability than YAG:Ce^{3+} [9]. The position of the Ce^{3+} 5d configuration is strongly influenced by the host lattice selection [10–13]. For the garnet structure, it can be presented by the general formula of $C_3A_2D_3O_{12}$, where C, A and D are dodecahedral, octahedral and tetrahedral sites with coordination numbers (CNs) of 8, 6 and 4, respectively [14]. It is well known that the garnet is quite flexible and can incorporate various cations into the C, A and D sites. This affords an opportunity to control the position of the Ce^{3+} $4f\rightarrow5d$ excitation and $5d\rightarrow4f$ emission bands by careful substitutions on the dodecahedral, octahedral and tetrahedral sites, because the lowest 5d excited state is strongly influenced by the site size and type coordinating Ce^{3+} [10–13]. In 2008, Shimomura et al. [15] performed a remarkable red shift by partially incorporating Mg^{2+} into the octahedral Sc^{3+} site to obtain a yellow-emitting phosphor $Ca_3ScMgSi_3O_{12}:Ce^{3+}$, which contained pronounced by-products of $Ca_2MgSi_2O_7$ and $CaMgSiO_4$. In 2011, we provided an effective means of achieving enhanced quality performance of the yellow $[Ca_{3-(x+0.06)}Lu_xCe_{0.06}](Sc_{2-y}Mg_y)Si_3O_{12}$ phosphor by eliminating the by-products through the introduction of Lu^{3+} at the Ca^{2+} site to compensate for the negative charge caused by the Mg^{2+} replacement for Sc^{3+} [16].

In this paper, we discuss the effect of charge balance on the crystal structure and optical properties of $[Ca_{3-(x+0.06)}Lu_xCe_{0.06}](Sc_{2-y}Mg_y)Si_3O_{12}$. After analyzing the change of bond length and covalency, the factors that determine crystal field splitting and centroid shift of Ce^{3+} 5d configurations, we provide an initial interpretation for the shift of Ce^{3+} emission and excitation when Lu^{3+} and Mg^{2+} are incorporated into CSS:Ce^{3+} as well as the thermal quenching mechanisms, and provide an optimization method for phosphors used for pcWLEDs.

2. Experimental

Samples with the general formula of $[Ca_{3-(x+0.06)}Lu_xCe_{0.06}](Sc_{2-y}Mg_y)Si_3O_{12}$ with $0\le x\le0.94$ and $0\le y\le1$ were prepared

* Corresponding authors. Tel./fax: +86 431 86708875.
E-mail address: zhangjh@ciomp.ac.cn (J. Zhang).

0022-2313/$ - see front matter © 2011 Elsevier B.V. All rights reserved.
doi:10.1016/j.jlumin.2011.12.060

by solid-state reactions. The raw materials of high purity $CaCO_3$, Lu_2O_3, CeO_2, Sc_2O_3, MgO and SiO_2 were homogenized according to stoichiometric proportions and fired in a tubular furnace under reducing conditions of 5% H_2+95% N_2 at 1200–1400 °C for 4 h. All samples were doped with 6 mol% Ce^{3+}. The structures of sintered samples were identified over the scattering range of $20^\circ \le 2\theta \le 60^\circ$ by X-ray powder diffractometer (XRD) (Rigaku D/M AX-2500V). The photoluminescence (PL) and photoluminescence excitation (PLE) spectra were measured using a Hitachi F4500 fluorescent spectrometer.

3. Results and discussion

3.1. Lu^{3+} incorporated CSS:Ce^{3+}

Fig. 1 shows the XRD patterns for samples with the nominal compositions of $[Ca_{3-(x+0.06)}Lu_xCe_{0.06}]Sc_2Si_3O_{12}$ (x=0.14, 0.34, 0.54, 0.74 and 0.94). For the lower Lu^{3+} content (x=0.14), one can see the primary phase is CSS (JCPDF no. 72-1969) with a few amount of by-products of Sc_2O_3 (JCPDF no. 74-1210) and SiO_2 (JCPDF no. 86-2327) phases. With the increasing Lu^{3+} contents ($x > 0.14$), however, possible additional by-products of $Lu_2Si_2O_7$ (JCPDF no. 35-0326), $Sc_2Si_2O_7$ (JCPDF no. 74-0989) and $Ce_2Si_2O_7$ (JCPDF no. 48-0058) appear and increase. For the higher Lu^{3+} contents (x=0.74 and 0.94), the amount of the by-products is significant. This indicates a limited solid solubility of Lu^{3+} on the dodecahedral sites. It can also be carefully observed that the XRD peaks shift to high angle regions with increasing x, reflecting the substitution of Ca^{2+} by Lu^{3+} for the ionic radius (r) of Lu^{3+} (r=0.977 Å for CN=8) is much smaller than that of Ca^{2+} (r=1.12 Å for CN=8) so as to shrink the lattice. It should be noted that the shrinkage of the lattice does not exclude the possibility of the Lu^{3+} substitution for Sc^{3+}. This is because the difference between the ionic radius of Lu^{3+} (r=0.861 Å for CN=6) and Sc^{3+} (r=0.745 Å for CN=6) is (0.116 Å) smaller than that (0.143 Å) between Lu^{3+} and Ca^{2+}. A minor substitution of Sc^{3+} by the larger Lu^{3+} cannot result in a macroscopic lattice expansion in case of a major substitution of Ca^{2+} by the smaller Lu^{3+}. The Lu^{3+} substitution for Sc^{3+} can be actually found from the by-products. The substitution of Sc^{3+} by Lu^{3+} leads to the residue of Sc^{3+}, consequently resulting in the formation of $Sc_2Si_2O_7$. The observation of $Lu_2Si_2O_7$ and $Sc_2Si_2O_7$ strongly indicates the limited solid solubility of Lu^{3+} in CSS in the case of charge mismatches between Lu^{3+} and Ca^{2+}.

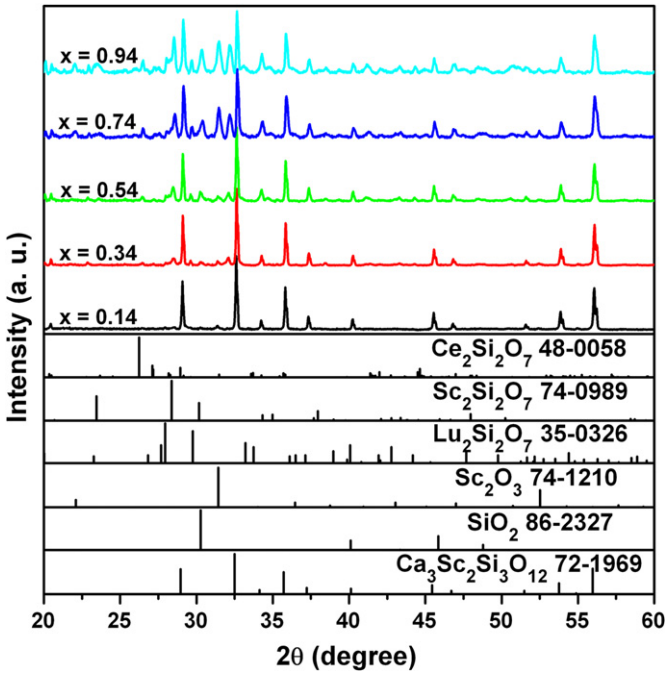

Fig. 1. XRD patterns for the samples of $[Ca_{3-(x+0.06)}Lu_xCe_{0.06}]Sc_2Si_3O_{12}$ (x=0.14, 0.34, 0.54, 0.74 and 0.94).

Fig. 2 shows the PL and PLE spectra of $[Ca_{3-(x+0.06)}Lu_xCe_{0.06}]Sc_2Si_3O_{12}$ (x=0, 0.14, 0.34, 0.54, 0.74 and 0.94). For x=0 (CSS:Ce^{3+}), the PL spectrum exhibits an intense green emission band peaked at 505 nm with a shoulder around 540 nm, originating from the transition from 5d to $^2F_{5/2}$ and $^2F_{7/2}$ of Ce^{3+}, respectively [9]. Meanwhile, the PLE spectrum for the green emission exhibits an intense excitation band around 450 nm and some weak bands in the UV region. Following the increased incorporation of Lu^{3+} into CSS:Ce^{3+}, the emission intensity dramatically drops off, which is correlated to the decrease of the CSS phase and the increase of the by-products phase. On the other hand, the PL spectra gradually shift to shorter wavelengths from 505 nm for x=0 to 499 nm for x=0.94 as well as the blue shift of the PLE spectra. To understand this phenomenon, the luminescences of the secondary silicate phases are analyzed. Ce^{3+}-doped silicates, such as $Re_2Si_2O_7$ (Re=Lu and Sc) that are present as the secondary phases in these samples, always have absorptions in the UV region and give rise to blue emissions [17]. Pauwels et al. have reported that $Lu_2Si_2O_7$:Ce^{3+} showed two excitation bands peaking at 305 and 355 nm and one emission band peaking at 380 nm [17]. Therefore, under 450 nm excitation, the emission bands of CSS:Ce^{3+} should not be influenced by $Lu_2Si_2O_7$:Ce^{3+}. Under UV excitation, the luminescence of these second phases could be re-absorbed by CSS:Ce^{3+}, consequently leading to unresolved excitation bands in the UV region other than in the blue (450 nm) region.

The position of the excitation and emission bands for Ce^{3+} in different hosts can be understood by analyzing two independent competing factors: the crystal field splitting of the 5d levels and the centroid shift of the 5d configuration with respect to the free ion position of the 5d levels [10–13]. Phenomenologically (or typically), the two factors are inversely dependent upon the Ce^{3+}–O^{2-} bond length. With the replacement of Ca^{2+} by smaller Lu^{3+}; however, the blue shift of emission and excitation does not follow the typical relationship between the bond length and the position of the lowest 5d excited state of Ce^{3+}. In this case, covalency and polarizability of Ce^{3+}-ligand bonds responsible for the centroid shift should play an important role in the blue shift

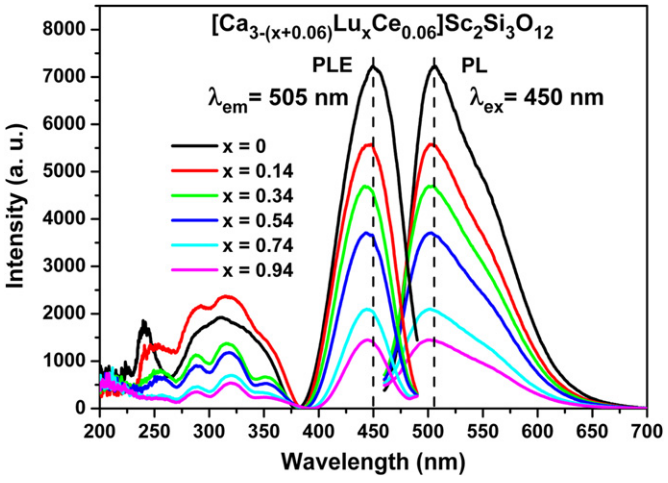

Fig. 2. PL (λ_{ex}=450 nm) and PLE (λ_{em}=505 nm) spectra for $[Ca_{3-(x+0.06)}Lu_xCe_{0.06}]Sc_2Si_3O_{12}$ (x=0, 0.14, 0.34, 0.54, 0.74 and 0.94).

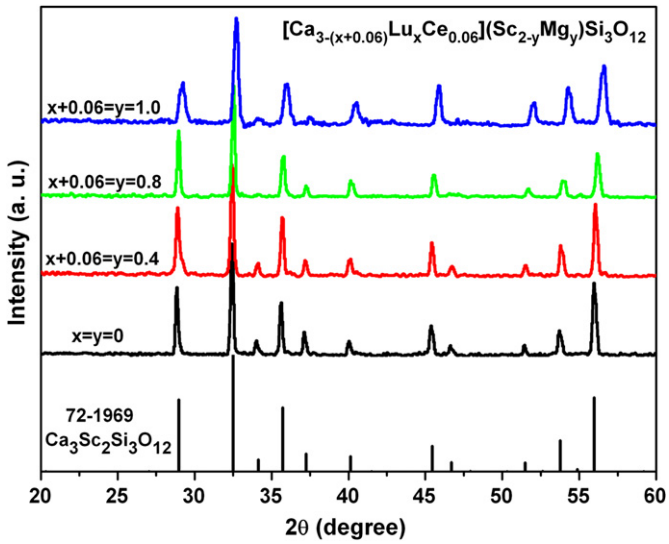

Fig. 3. XRD patterns for the samples of $[Ca_{3-(x+0.06)}Lu_xCe_{0.06}](Sc_{2-y}Mg_y)Si_3O_{12}$ (x=0, 0.34, 0.74, 0.94 and y=0, 0.4, 0.8, 1.0).

behavior. For Lu^{3+} the anion polarizability is smaller than that for Ca^{2+} because of the larger electronegativity of Lu^{3+} (χ(Lu)=1.27) than that of Ca^{2+} (χ(Ca)=1.00). This means that the bonding of the valence electron of oxygen to Lu^{3+} increases. In other words, the ionicity of the Lu^{3+}–O^{2-} bond decreases while the covalency of Lu^{3+}–O^{2-} bond increases, thereby decreasing the covalency of Ce^{3+}–O^{2-} bond and resulting in a smaller centroid shift of the 5d levels from the free Ce^{3+} ion levels. The effect of centroid shift is more pronounced than that of the crystal field splitting. Therefore, the blue shift of the emission and excitation is observed. After analyzing the two factors, it is noticed that polarizability (or electronegativity) plays a more effective role than bond lengths.

3.2. Lu^{3+}–Mg^{2+} incorporated CSS:Ce^{3+}

Fig. 3 shows the XRD patterns for the phosphors with nominal compositions of $[Ca_{3-(x+0.06)}Lu_xCe_{0.06}](Sc_{2-y}Mg_y)Si_3O_{12}$ with x=0, 0.34, 0.74, 0.94 and y=0, 0.4, 0.8, 1.0. All the samples exhibit a pure CSS phase, which are greatly different from the case of Lu^{3+} or Mg^{2+} single doped CSS:Ce^{3+}. Meanwhile, it is obvious that the XRD peaks shift to larger angle regions, indicating a decrease of the lattice parameter. This phenomenon accords with the replacements of Ca^{2+} by Lu^{3+} and Sc^{3+} by Mg^{2+}, because both the ionic radius of Lu^{3+} (r=0.977 Å for CN=8) and Mg^{2+} (r=0.72 Å for CN=6) are smaller than that of Ca^{2+} (r=1.12 Å for CN=8) and Sc^{3+} (r=0.745 Å for CN=6), respectively. Lattice parameters were calculated according to the XRD data in Fig. 3 using Jade 5. As Fig. 4 presents, the lattice parameters against the Lu^{3+} and/or Mg^{2+} contents follow Vegard's law, reflecting a complete solid solution of Lu^{3+} and Mg^{2+} in CSS in the case of charge balance of the total molecular formula.

Shimomura et al. have reported that abundant by-products of $Ca_2MgSi_2O_7$ and $CaMgSiO_4$ appeared when Mg^{2+} was singly present at the Sc^{3+} site in CSS:Ce^{3+}[15]. In Section 3.1, we also demonstrate that large by-products are formed when Lu^{3+} is singly present at the Ca^{2+} site. Charge mismatches between Mg^{2+} and Sc^{3+} or between Lu^{3+} and Ca^{2+} should answer for the two cases, respectively. Keeping the content of Mg^{2+} on the Sc^{3+} site while enhancing the content of Lu^{3+} on the Ca^{2+} site, the phases of $Ca_2MgSi_2O_7$ and $CaMgSiO_4$ gradually disappeared and a pure CSS phase was obtained when the charge of the total molecular formula reached a balance [16]. Therefore, it is concluded that charge balance of the total molecular formula plays

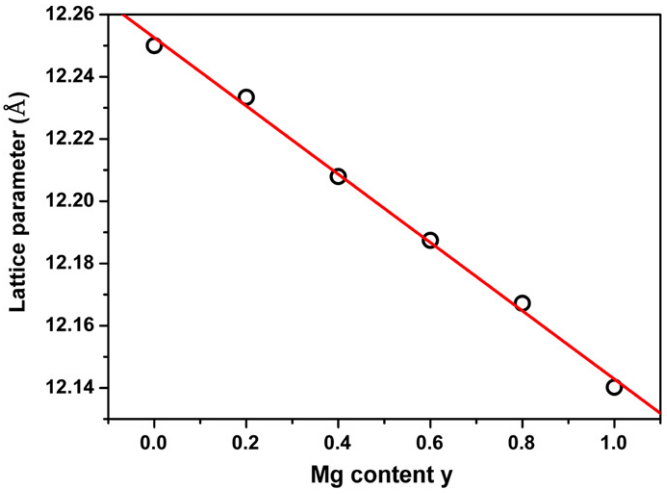

Fig. 4. Lattice parameters against Mg content for $[Ca_{3-(x+0.06)}Lu_xCe_{0.06}]$–$(Sc_{2-y}Mg_y)Si_3O_{12}$ with x=0, 0.14, 0.34, 0.54, 0.74, 0.94 and y=0, 0.2, 0.4, 0.6, 0.8, 1.0.

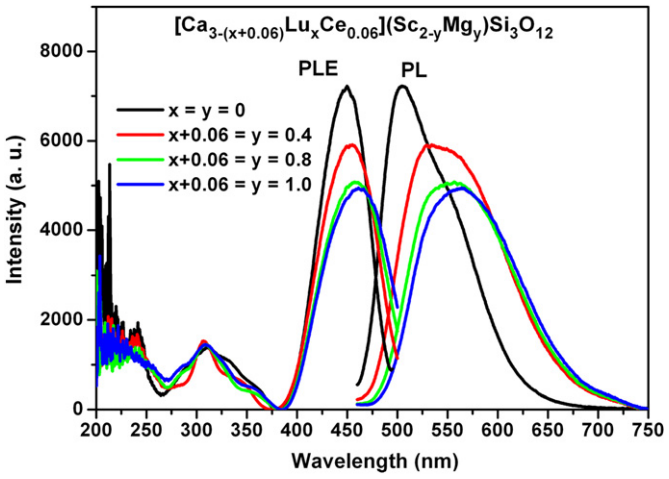

Fig. 5. PL (λ_{ex}=450 nm) and PLE (monitored at the emission maximum wavelength) spectra for $[Ca_{3-(x+0.06)}Lu_xCe_{0.06}](Sc_{2-y}Mg_y)Si_3O_{12}$ (x=0, 0.34, 0.74, 0.94 and y=0, 0.4, 0.8, 1.0).

an important role in the garnet phase formation. In 2006, Setlur et al. [18] reported a red-emitting silicate garnet $Lu_2CaMg_2Si_3O_{12}$:Ce^{3+} phosphor. A complete solid solution between the two silicate garnets CSS and $Lu_2CaMg_2Si_3O_{12}$ was demonstrated by the same authors in 2010 [19]. In this paper, we achieve a similar result. However, the effects of Lu^{3+} and those of Mg^{2+} on the luminescence properties are different from each other and specified in this report.

Fig. 5 shows the PL and PLE spectra for $[Ca_{3-(x+0.06)}Lu_xCe_{0.06}](Sc_{2-y}Mg_y)Si_3O_{12}$ with x=0, 0.34, 0.74, 0.94 and y=0, 0.4, 0.8, 1.0. The PL spectra were excited by 450 nm and the PLE spectra were monitored at the emission peak wavelength. With the increasing Lu^{3+} and Mg^{2+} contents, the emission shifts to longer wavelengths from 505 nm (y=0) to 560 nm (y=1) following a peak intensity decrease as well as the excitation. However, the integral intensity is almost unchanged, reflecting the unchanged quantum efficiency (QE) at room temperature.

Shimomura et al. [15] have demonstrated that the red shift of the emission spectra of the Mg^{2+} single doped CSS:Ce^{3+} was caused by the enhanced Ce^{3+} content for charge compensation effects. Whereas, differing from the almost unchanged excitation spectra for the Mg^{2+} single doped CSS:Ce^{3+}, the excitation for the

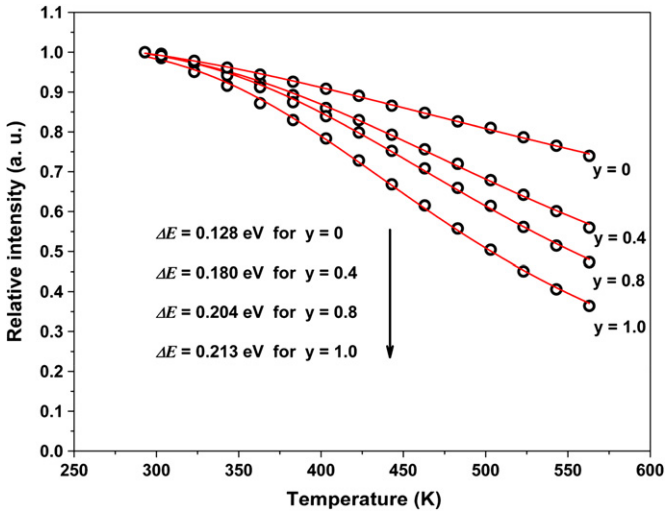

Fig. 6. PL intensity versus temperature for $[Ca_{3-(x+0.06)}Lu_xCe_{0.06}](Sc_{2-y}Mg_y)Si_3O_{12}$ (x=0, 0.34, 0.74, 0.94 and y=0, 0.4, 0.8, 1.0) under 450 nm excitation. The circles are experimental data and the lines are the fitting functions.

Lu^{3+} and Mg^{2+} double doped CSS:Ce^{3+} exhibits a red shift. Considering the two factors of crystal field splitting and centroid shift aforementioned, the changes of bond length and covalency are analyzed. As Fig. 4 depicts, the reduction of the lattice parameters indicates a shorter Ce^{3+}–O^{2-} bond for the compression of the garnet, shifting the lowest excited 5d state energy level of Ce^{3+} to an even lower energy position for the stronger crystal field splitting. This regular result is similar to that from $Lu_2CaMg_2Si_3O_{12}$ to CSS reported by Setlur et al., who demonstrated a smaller crystal field splitting from the longer Ce^{3+}–O^{2-} bond length [19]. Furthermore, the electronegativity of Mg^{2+} (χ(Mg)=1.31) is smaller than that of Sc^{3+} (χ(Sc)=1.36), which means a higher ionicity of the Mg^{2+}–O^{2-} bond and a more covalent Ce^{3+}–O^{2-} bond. Therefore, a lower energy position of the lowest 5d excited state is induced for a larger centroid shift arising from the higher covalent Ce^{3+}–O^{2-} bond. This is also demonstrated by the larger Ce^{3+} centroid shift in $Lu_2CaMg_2Si_3O_{12}$ ($\sim$13,300 cm^{-1}) than that in CSS ($\sim$12,300 cm^{-1}) [19]. Taking the stronger crystal field splitting effect and the larger centroid shift into account, a lower energy Ce^{3+} 4f→5d excitation and 5d→4f emission band is observed. After estimating the effect of Lu^{3+} and Mg^{2+}, the red shift of the emission and excitation should be attributed to Mg^{2+} other than to Lu^{3+} inducing a blue shift as discussed in Section 3.1. However, Lu^{3+} also plays an important role in the enhancements of luminescence intensity and thermal stability [16].

With the incorporation of Lu^{3+} and Mg^{2+} into CSS:Ce^{3+}, the QE at room temperature is almost unchanged. However, as shown in Fig. 6, the QE significantly reduces at high temperature. The energy difference between the excited 5d state and the bottom of the conduction band is named activation energy (ΔE). The smaller the activation energy, the stronger the thermal quenching. Using the equation of $I(T)=I(0)/(1+A\exp(-\Delta E/k_BT))$ with constant A and Boltzmann constant k_B, the activation energies were estimated to be 0.128, 0.180, 0.204 and 0.213 eV for y=0, 0.4, 0.8 and 1.0, respectively. Apparently, the result of the increase ΔE with the increasing value of y is opposite to the thermal quenching behavior. This could be related with the smaller temperature range that leads to an inexact activation energy. On the other hand, basing on the configurational coordinate diagram [20], thermal quenching is described as a nonradiative relaxation process between the lowest excited 5d state and the 4f ground state. A larger Stokes shift induces a lower energy barrier for nonradiative relaxation processes and results in a stronger thermal quenching. Stokes shift can be obtained from the energy difference between the lowest excitation peak and the higher emission peak. From the room temperature spectra (Fig. 5) the Stokes shifts are calculated to be 2470, 2850, 2900 and 2930 cm^{-1} for y=0, 0.4, 0.8 and 1.0, respectively. Combining the discussions above, the increased Stokes shift should respond to the stronger thermal quenching with increasing Lu^{3+} and Mg^{2+} substitutions.

4. Conclusions

In summary, we demonstrate that charge balance plays an important role in the CSS garnet structure formation for the Lu^{3+} and Mg^{2+} incorporated $[Ca_{3-(x+0.06)}Lu_xCe_{0.06}]$–$(Sc_{2-y}Mg_y)Si_3O_{12}$ with $0\le x\le 0.94$ and $0\le y\le 1$. The changes of bond and covalence are analyzed when Lu^{3+} and Mg^{2+} are introduced into CSS. The shift of Ce^{3+} emission and excitation can be attributed to the result from the combined effect of crystal field splitting and centroid shift of Ce^{3+} 5d levels. The decrease of the QE at high temperature is induced by the nonradiative relaxation processes according to the configurational coordinate diagram. Understanding the factors that influence the position of Ce^{3+} emission and excitation as well as the thermal quenching mechanisms provide an optimization method for phosphors used for pcWLEDs.

Acknowledgments

This work is financially supported by the National Nature Science Foundation of China (10834006, 10904141, 10904140, 51172226, 11174278), the MOST of China (2010AA03A404).

References

[1] S. Nakamura, T. Mukai, M. Senoh, Appl. Phys. Lett. 64 (1994) 1687.
[2] E.F. Schubert, J.K. Kim, Science 308 (2005) 1274.
[3] S. Nakamura, Proc. SPIE 3002 (1997) 26.
[4] K. Bando, K. Sakano, Y. Noguchi, Y. Shimizu, J. Light Visual Environ. 22 (1998) 2.
[5] G. Blasse, A. Bril, J. Chem. Phys. 47 (1967) 5139.
[6] W.W. Holloway Jr., M. Kestiglan, J. Opt. Soc. Am. 59 (1969) 60.
[7] T.Y. Tien, E.F. Gibbons, R.G. Delosh, P.J. Zacmanidis, D.E. Smith, H.L. Stadler, J. Electrochem. Soc. 120 (1973) 278.
[8] A.A. Setlur, A.M. Srivastava, H.A. Comanzo, G. Chandran, H. Aiyer, M.V. Shankar, S.E. Weaver, Proc. SPIE 5187 (2004) 142.
[9] Y. Shimomura, T. Honma, M. Shigeiwa, T. Akai, K. Okamoto, N. Kijima, J. Electrochem. Soc. 154 (2007) J35.
[10] P. Dorenbos, Phys. Rev. B 64 (2001) 125117.
[11] P. Dorenbos, Phys. Rev. B 65 (2002) 235110.
[12] P. Dorenbos, J. Lumin. 99 (2002) 283.
[13] P. Dorenbos, J. Lumin. 105 (2003) 117.
[14] S. Geller, Z. Kristallogr. 125 (1967) 1.
[15] Y. Shimomura, T. Kurushima, M. Shigeiwa, N. Kijima, J. Electrochem. Soc. 155 (2008) J45.
[16] Y.F. Liu, X. Zhang, Z.D. Hao, W. Lu, X.Y. Liu, X.J. Wang, J.H. Zhang, J. Phys. D: Appl. Phys. 44 (2011) 075402.
[17] D. Pauwels, N. le Masson, B. Vianan, A. Kahn-Harari, E.V.D. van Loef, P. Dorenbos, C.W.E. van Eijk, IEEE Trans. Nucl. Sci. 47 (2000) 1787.
[18] A.A. Setlur, W.J. Heward, Y. Gao, A.M. Srivastava, R.G. Chandran, M.V. Shankar, Chem. Mater. 18 (2006) 3314.
[19] M.S. Kishore, N.P. Kumar, R.G. Chandran, A.A. Setlur, Electrochem. Solid-State Lett. 13 (2010) J77.
[20] C.C. Chiang, M.S. Tsai, M.H. Hon, J. Electrochem. Soc. 155 (2008) B517.